An Equilibrated Error Estimator for the 2-D/1-D MSFEM T-Formulation of the Eddy Current Problem

Markus Schöbinger and Karl Hollaus

Institute for Analysis and Scientific Computing, Technische Universität Wien, 1040 Vienna, Austria

The 2-D/1-D multiscale finite element method (MSFEM) is an efficient way to simulate rotating machines in which each iron sheet is exposed to the same field. It allows the reduction of the 3-D sheet to a 2-D cross section by resolving the dependence along the thickness of the sheet with a polynomial expansion. This work presents an equilibrated error estimator based on flux equilibration and the theorem of Prager and Synge for the T-formulation of the eddy current problem in a 2-D/1-D MSFEM setting. The estimator is shown to give both a good approximation of the total error and to allow for adaptive mesh refinement by correctly estimating the local error distribution.

***Index Terms*— 2-D/1-D multiscale finite element method (MSFEM), eddy currents, error estimator.**

I. Introduction

THE simulation of eddy currents in electrical machines consisting of many steel sheets with the finite element method quickly leads to infeasibly large equation systems. In many machines, each sheet in the active zone is exposed to the same field, which allows for a great reduction in computational effort by simulating only a single sheet. If required, the effect of the end-winding reason can be included via a network equation as has been done in [1].

However, this reduced problem is still far from trivial. One method to further simplify the problem while maintaining a good approximation of the solution is by spacial decomposition.

The thickness of one sheet is less than a millimeter while the length and width are in the range of meters. A method to treat the 2-D cross section and the 1-D thickness of the sheet as two coupled problems has been presented in [2]. It solves the two problems iteratively until convergence is reached. The nature of this coupling has been analyzed in more detail in [3].

In [4] and [5] different approaches have been presented which isolate the 1-D problem as a pre-processing step in order to obtain parameters for the 2-D one.

The 2-D/1-D multiscale finite element method (MSFEM) presented in [6] applies ideas from the MSFEM. It uses classic finite element functions for the 2-D problem while approximating the dependence on the third axis with pre-defined polynomial shape functions. The idea is similar to the method presented in [7], which is based on trigonometrical shape functions. This enables the solution of the problem within a single iteration while requiring only a mesh for the 2-D cross section of the sheet. It is also able to include the insulation layers between sheets and correctly treat the edge effect [8].

Manuscript received 3 February 2023; revised 26 April 2023, 22 June 2023, and 4 December 2023; accepted 27 February 2024. Date of publication 4 March 2024; date of current version 25 April 2024. Corresponding author: M. Schöbinger (e-mail: markus.schoebinger@tuwien.ac.at).

Color versions of one or more figures in this article are available at https://doi.org/10.1109/TMAG.2024.3372705.

Digital Object Identifier 10.1109/TMAG.2024.3372705

This article presents an error estimator for the **T**-formulation of the 2-D/1-D MSFEM. It is based on flux equilibration and similar to the error estimator for the **T**-formulation for the MSFEM presented in [9]. The theory has been restructured in order to fit within the 2-D/1-D MSFEM framework. Both the construction and the evaluation of the presented estimator require only the 2-D mesh while being valid in the complete 3-D domain.

A numerical example shows that the estimator gives a good approximation of the error in both a global and a local sense. This latter property is used to implement adaptive mesh refinement. This allows for a high accuracy of the 2-D/1-D MSFEM solution while requiring significantly fewer degrees of freedom than uniform mesh refinement.

II. T–Φ-Formulation

We use the **T**–Φ formulation for the reference solution of the eddy current problem as described in [10]. The problem domain Ω is split into the conducting domain Ω_c, consisting of the steel sheet, and the non-conducting domain Ω_0, consisting of the air regions and the insulation layers. The sheet is assumed to be axis-aligned with the cross section in the x-y plane and the thickness aligned with the z-axis. The total thickness of Ω is $d = d_{\mathrm{Fe}} + d_0$ with the thickness of the sheet d_{Fe} and the thickness of the insulation layer d_0.

The magnetic field strength $\mathbf{H}$ is written as

$$\mathbf{H} = \mathbf{T} - \nabla\Phi + \mathbf{H}_{\mathrm{BS}} \tag{1}$$

with the current vector potential $\mathbf{T} \in H(\mathrm{curl}, \Omega_c)$ fulfilling $\mathrm{curl}\,\mathbf{T} = \mathbf{J}$ with the current density $\mathbf{J}$, the magnetic scalar potential $\Phi \in H^1(\Omega)$ and a prescribed Biot-Savart field $\mathbf{H}_{\mathrm{BS}}$. The strong formulation of the eddy current problem in the frequency domain is given as

$$\mathrm{curl}\,\rho\,\mathrm{curl}\,\mathbf{T} + i\omega\mu(\mathbf{T} - \nabla\Phi + \mathbf{H}_{\mathrm{BS}}) = \mathbf{0} \tag{2}$$

where $\rho = \sigma^{-1}$ is the electric resistivity with the electric conductivity σ, μ is the magnetic permeability, $\omega = 2\pi f$ the angular frequency with the frequency f and i is the imaginary unit.

Multiplication with a test function and integration by parts, together with the auxiliary condition $\operatorname{div}\mathbf{B} = 0$ for the magnetic flux density $\mathbf{B} = \mu\mathbf{H}$, lead to the weak formulation: find $\mathbf{T} \in H(\operatorname{curl}, \Omega_c)$ and $\Phi \in H^1(\Omega)$ so that

$$\int_\Omega \rho \operatorname{curl}\mathbf{T} \cdot \operatorname{curl}\mathbf{v} + i\omega\mu(\mathbf{T} - \nabla\Phi) \cdot (\mathbf{v} - \nabla q) = -\int_\Omega i\omega\mu\mathbf{H}_{\mathrm{BS}} \cdot (\mathbf{v} - \nabla q) \quad (3)$$

for all $\mathbf{v} \in H(\operatorname{curl}, \Omega_c)$ and all $q \in H^1(\Omega)$.

III. Two-Dimensional/1-D MSFEM T-Formulation

This article uses the 2-D/1-D MSFEM approach for the **T**-formulation which has been described in detail in [6] and [11]. The 3-D unknown function $\mathbf{T} - \nabla\Phi$ is approximated by

$$\mathbf{T}_{\text{2-D/1-D}} = \begin{pmatrix} \phi_0(z)\mathbf{T}_{0,x}(x, y) + \phi_2(z)\mathbf{T}_{2,x}(x, y) \\ \phi_0(z)\mathbf{T}_{0,x}(x, y) + \phi_2(z)\mathbf{T}_{2,y}(x, y) \\ 0 \end{pmatrix} \quad (4)$$

where $\mathbf{T}_2 \in H(\operatorname{curl}_{\text{2-D}}, \Omega_{\text{2-D},c})$ and $\mathbf{T}_0 = \nabla\Phi_0$ with $\Phi_0 \in H^1(\Omega_{\text{2-D}})$ are defined on the 2-D projection $\Omega_{\text{2-D}}$ of Ω. Here and in the following, coordinates x, y or z in the index denote the individual components of a vector-valued function.

This article assumes that the sheets form closed loops with the magnetic field running parallel to them. Then, the dependence of **T** on z is an even function. This allows to drop the odd orders in a polynomial expansion.

The shape functions ϕ_0 and ϕ_2 are polynomial basis functions of order 0 and 2, respectively. They are chosen so that only ϕ_0 is non-zero on the boundaries of the sheets. More details about the definition of the shape functions can be found in Appendix.

The 2-D rotation operator $\operatorname{curl}_{\text{2-D}}$ of a 2-D vector function $\mathbf{V} = (\mathbf{V}_x(x, y), \mathbf{V}_y(x, y))^T$ is defined as

$$\operatorname{curl}_{\text{2-D}}\mathbf{V} := \frac{\partial}{\partial x}\mathbf{V}_y - \frac{\partial}{\partial y}\mathbf{V}_x. \quad (5)$$

The discretization of the space $H(\operatorname{curl}_{\text{2-D}})$ is discussed in detail in [12].

The full magnetic field strength is then given by

$$\mathbf{H}_{\text{2-D/1-D}} = \mathbf{T}_{\text{2-D/1-D}} + \mathbf{H}_{\mathrm{BS}}. \quad (6)$$

For later reference, the (3-D) rotation of $\mathbf{H}_{\text{2-D/1-D}}$ is given by

$$\operatorname{curl}\mathbf{H}_{\text{2-D/1-D}} = \begin{pmatrix} -\phi_2'(z)\mathbf{T}_{2,y}(x, y) \\ \phi_2'(z)\mathbf{T}_{2,x}(x, y) \\ \phi_2 \operatorname{curl}_{\text{2-D}}\mathbf{T}_2 \end{pmatrix}. \quad (7)$$

Note that the x and y components in (7) yield the laminar currents, while the z component is relevant for the edge effect where the currents change direction by flowing perpendicular to the sheet.

To obtain the weak formulation, (4) is used in (3) for both the trial function and the test function. Note that $\mathbf{H}_{\text{2-D/1-D}}$ only depends on z via the shape functions ϕ_0 and ϕ_2, which are known a priori. Therefore integration over z can be carried out analytically. This yields the weak 2-D/1-D MSFEM formulation: find $\mathbf{T}_2 \in H(\operatorname{curl}_{\text{2-D}}, \Omega_{\text{2-D},c})$ and $\Phi_0 \in H^1(\Omega_{\text{2-D}})$ so that

$$\begin{aligned} \int_{\Omega_{\text{2-D}}} & \overline{\rho\phi_2'^2}\mathbf{T}_2 \cdot \mathbf{V}_2 + \overline{\rho\phi_2^2} \operatorname{curl}_{\text{2-D}}\mathbf{T}_2 \operatorname{curl}_{\text{2-D}}\mathbf{V}_2 \\ & + i\omega\left(\overline{\mu\phi_0^2}\nabla\Phi_0 \cdot \nabla q + \overline{\mu\phi_2^2}\mathbf{T}_2 \cdot \mathbf{V}_2\right) \\ & + i\omega\overline{\mu\phi_0\phi_2}(\nabla\Phi_0 \cdot \mathbf{V}_2 + \mathbf{T}_2 \cdot \nabla q) \\ = & -\int_{\Omega_{\text{2-D}}} i\omega\left(\overline{\mu\phi_0^2}\mathbf{H}_{\mathrm{BS}} \cdot \nabla q + \overline{\mu\phi_0\phi_2}\mathbf{H}_{\mathrm{BS}} \cdot \mathbf{V}_2\right) \end{aligned} \quad (8)$$

for all $\mathbf{V}_2 \in H(\operatorname{curl}_{\text{2-D}}, \Omega_{\text{2-D},c})$ and $q \in H^1(\Omega_{\text{2-D}})$ where a bar denotes that the respective function has been integrated with respect to z. All pre-computed integrals appearing in this article are given in Appendix.

IV. Error Estimation

The proposed error estimator is based on the theorem of Prager and Synge and the theory presented in [13]. These results can be adapted to obtain the following identity which is the basis for all further calculations:

$$\|\operatorname{curl}\mathbf{T} - \operatorname{curl}\mathbf{T}_{\text{2-D/1-D}}\|_\rho^2 + \|\sigma\gamma - \operatorname{curl}\mathbf{T}\|_\rho^2 = \|\sigma\gamma - \operatorname{curl}\mathbf{T}_{\text{2-D/1-D}}\|_\rho^2 \quad (9)$$

where **T** is the strong solution of the eddy current problem (2) and γ an equilibrated flux fulfilling the condition

$$\operatorname{curl}\gamma = -i\omega\mu(\mathbf{T}_{\text{2-D/1-D}} + \mathbf{H}_{\mathrm{BS}}). \quad (10)$$

The energy norm $\|\cdot\|_\rho$ can be interpreted as a measurement for the eddy current losses, i.e., for the current density **J** there holds

$$\|\mathbf{J}\|_\rho^2 = \int_\Omega \rho\mathbf{J} \cdot \mathbf{J}^* = \int_\Omega \mathbf{E} \cdot \mathbf{J}^* \quad (11)$$

where the asterisk denotes the complex conjugate.

The main idea of the theorem of Prager and Synge is to see γ as a second numerical electric field strength, in addition to $\rho\operatorname{curl}\mathbf{T}_{\mathrm{BS}}$. Using its definition (10) it can be shown that the error of $\sigma\gamma$ is orthogonal to the error of $\operatorname{curl}\mathbf{T}_{\mathrm{BS}}$ in the scalar product inducing the energy norm. In this sense, (9) simply becomes the Pythagorean theorem.

In (9), the first term is the error we are interested in. Assuming a suitable γ is known, the right-hand side of (9) can be calculated. Because the error with respect to $\sigma\gamma$ is non-negative, the right-hand side is guaranteed to provide an upper bound for the error.

A variant of (9) for the 2-D scalar **T**-formulation has been proven in [9] and for the vector-valued magnetostatic case in [13]. The proof of (9) is analogous.

The main problem is the construction of a suitable γ which needs to fulfill (10) on Ω. At the same time, it needs to be able to be constructed using only $\Omega_{\text{2-D}}$. If the error estimator required the full 3-D domain Ω, it would be much more computationally expensive than the calculation of $\mathbf{T}_{\text{2-D/1-D}}$ and nullify the advantages of using a 2-D/1-D MSFEM. Similarly, the evaluation of the estimator, as defined by the 3-D integral on the right-hand side of (9), needs to be doable using only $\Omega_{\text{2-D}}$.

This is achieved by using a 2-D/1-D MSFEM approach for γ as well. More specifically, we set

$$\gamma = \begin{pmatrix} \hat{\phi}_1(z)\gamma_{1,x}(x,y) + \hat{\phi}_3(z)\gamma_{3,x}(x,y) \\ \hat{\phi}_1(z)\gamma_{1,y}(x,y) + \hat{\phi}_3(z)\gamma_{3,y}(x,y) \\ \phi_0(z)\gamma_{0,y}(x,y) + \phi_2(z)\gamma_{2,y}(x,y) \end{pmatrix} \tag{12}$$

with

$$\hat{\phi}_1 := \int \phi_0 \, dz \quad \text{and} \quad \hat{\phi}_3 := \int \phi_2 \, dz \tag{13}$$

and the unknowns $\gamma_0, \gamma_2 \in H^1(\Omega_{2\text{-D}})$ and $\gamma_1, \gamma_3 \in H(\operatorname{curl}_{2\text{-D}}, \Omega_{2\text{-D}})$ to be determined.

Note that both terms in the estimator on the right-hand side of (9) are equal to zero inside the insulation. For $\sigma\gamma$ this holds because of the multiplication with the conductivity. For the second term $\operatorname{curl} \mathbf{T}_{2\text{-D/1-D}}$, all its components contain the shape function ϕ_2, see (7), which is also set to zero inside the insulation. Therefore it suffices to consider only the domain of the conducting material for the construction γ, i.e., $\gamma_0, \gamma_2 \in H^1(\Omega_{2\text{-D},c})$ and $\gamma_1, \gamma_3 \in H(\operatorname{curl}_{2\text{-D}}, \Omega_{2\text{-D},c})$. A consequence of this is, that $\phi_2' = K\hat{\phi}_1$ holds with the constant $K = 2\sqrt{6}/d_{\text{Fe}}^2$.

The rotation of γ is given by

$$\operatorname{curl}\gamma = \begin{pmatrix} \phi_0 \dfrac{\partial}{\partial y}\gamma_0 - \phi_0\gamma_{1,y} + \phi_2 \dfrac{\partial}{\partial y}\gamma_2 - \phi_2\gamma_{3,y} \\ \phi_0\gamma_{1,x} - \phi_0 \dfrac{\partial}{\partial x}\gamma_0 + \phi_2\gamma_{3,x} - \phi_2 \dfrac{\partial}{\partial x}\gamma_2 \\ \hat{\phi}_1 \operatorname{curl}_{2\text{-D}} \gamma_1 + \hat{\phi}_3 \operatorname{curl}_{2\text{-D}} \gamma_3 \end{pmatrix}. \tag{14}$$

The condition (10) is written out, using both (4) and (14). Comparing the coefficients with respect to the shape functions yields the equations

$$\frac{\partial}{\partial y}\gamma_0 - \gamma_{1,y} = -i\omega\mu\left(\mathbf{T}_{0,x} + \mathbf{H}_{\text{BS},x}\right) \tag{15}$$

$$\frac{\partial}{\partial y}\gamma_2 - \gamma_{3,y} = -i\omega\mu\mathbf{T}_{2,x} \tag{16}$$

$$\gamma_{1,x} - \frac{\partial}{\partial x}\gamma_0 = -i\omega\mu\left(\mathbf{T}_{0,y} + \mathbf{H}_{\text{BS},y}\right) \tag{17}$$

$$\gamma_{3,x} - \frac{\partial}{\partial x}\gamma_2 = -i\omega\mu\mathbf{T}_{2,y} \tag{18}$$

$$\operatorname{curl}_{2\text{-D}} \gamma_1 = 0 \tag{19}$$

$$\operatorname{curl}_{2\text{-D}} \gamma_3 = 0. \tag{20}$$

From (19) and (20) it follows that $\gamma_1 = \nabla\Phi_1$ and $\gamma_3 = \nabla\Phi_3$ with $\Phi_1, \Phi_3 \in H^1(\Omega_{2\text{-D},c})$. With this, the remaining equations can be rewritten as

$$\begin{pmatrix} \dfrac{\partial}{\partial y}\gamma_0 - \dfrac{\partial}{\partial y}\Phi_1 \\ \dfrac{\partial}{\partial x}\Phi_1 - \dfrac{\partial}{\partial x}\gamma_0 \end{pmatrix} = -i\omega\mu(\mathbf{T}_0 + \mathbf{H}_{\text{BS}}) \tag{21}$$

$$\begin{pmatrix} \dfrac{\partial}{\partial y}\gamma_2 - \dfrac{\partial}{\partial y}\Phi_3 \\ \dfrac{\partial}{\partial x}\Phi_3 - \dfrac{\partial}{\partial x}\gamma_2 \end{pmatrix} = -i\omega\mu\mathbf{T}_2. \tag{22}$$

Note that (21) and (22) do not uniquely define all components of γ. Every solution yields a valid error estimator, but the overestimation [given by the second term on the left-hand side of (9)] may become arbitrarily large. As can be seen from (9), minimizing the overestimation is equivalent to minimizing the estimator, because the error is independent of γ. For this purpose additional conditions are imposed.

Because the estimator is small if $\sigma\gamma$ is a good approximation of $\operatorname{curl}\mathbf{T}_{2\text{-D/1-D}}$, a comparison of (7) and (12) suggests that

$$\nabla\Phi_1 \approx K\rho\begin{pmatrix} -\mathbf{T}_{2,y} \\ \mathbf{T}_{2,x} \end{pmatrix} \tag{23}$$

$$\nabla\Phi_3 \approx \mathbf{0} \tag{24}$$

$$\gamma_0 \approx 0 \tag{25}$$

$$\gamma_2 \approx \rho \operatorname{curl}_{2\text{-D}} \mathbf{T}_2 \tag{26}$$

should hold.

In this article we solve (21) under the constraint

$$\|\sigma\gamma_0\|_\rho^2 + \left\|\sigma\hat{\phi}_1\nabla\Phi_1 - \phi_2'\begin{pmatrix} -\mathbf{T}_{2,y} \\ \mathbf{T}_{2,x} \end{pmatrix}\right\|_\rho^2 \to \min \tag{27}$$

and (22) under the constraint

$$\|\sigma\phi_2\gamma_2 - \phi_2 \operatorname{curl}_{2\text{-D}} \mathbf{T}_2\|_\rho^2 + \left\|\sigma\hat{\phi}_3\nabla\Phi_3\right\|_\rho^2 \to \min. \tag{28}$$

This does not yield the optimal minimizer of the estimator because the interdependence of the components is neglected. However, the numerical example shows that this suffices to achieve an acceptable amount of overestimation. The main advantage of this approach is that instead of one big minimization problem one only has to solve two smaller ones. This is both faster in itself and can even be done in parallel.

The weak formulation for the problem (21) and (27) reads as: find $\gamma_0, \Phi_1 \in H^1(\Omega_{2\text{-D},c})$ and a Lagrange multiplier $\lambda_1 \in H_\lambda(\Omega_{2\text{-D},c})$ so that

$$\begin{aligned} &\int_{\Omega_{2\text{-D},c}} \overline{\sigma\phi_0^2}\gamma_0\chi_0 + \overline{\sigma\hat{\phi}_1^2}\nabla\Phi_1\cdot\nabla\chi_1 \\ &\qquad + \lambda_1\cdot\begin{pmatrix} \dfrac{\partial}{\partial y}\chi_0 - \dfrac{\partial}{\partial y}\chi_1 \\ \dfrac{\partial}{\partial x}\chi_1 - \dfrac{\partial}{\partial x}\chi_0 \end{pmatrix} + \begin{pmatrix} \dfrac{\partial}{\partial y}\gamma_0 - \dfrac{\partial}{\partial y}\Phi_1 \\ \dfrac{\partial}{\partial x}\Phi_1 - \dfrac{\partial}{\partial x}\gamma_0 \end{pmatrix}\cdot\kappa_1 \\ &= \int_{\Omega_{2\text{-D}}} K\overline{\hat{\phi}_1^2}\begin{pmatrix} -\mathbf{T}_{2,y} \\ \mathbf{T}_{2,x} \end{pmatrix}\cdot\nabla\chi_1 - i\omega\mu(\mathbf{T}_0 + \mathbf{H}_{\text{BS}})\cdot\kappa_1 \end{aligned} \tag{29}$$

for all $\chi_0, \chi_1 \in H^1(\Omega_{2\text{-D},c})$ and $\kappa_1 \in H_\lambda(\Omega_{2\text{-D},c})$, where, according to the de Rham complex, the Lagrange multiplier space $H_\lambda(\Omega_{2\text{-D},c})$ is given as the space $H(\operatorname{div}, \Omega_{2\text{-D},c})$ restricted to divergence-free functions.

Similarly, the weak formulation for the problem (22) and (28) reads as: find $\gamma_2, \Phi_3 \in H^1(\Omega_{2\text{-D},c})$ and a Lagrange multiplier $\lambda_2 \in H_\lambda(\Omega_{2\text{-D},c})$ so that

$$\begin{aligned} &\int_{\Omega_{2\text{-D},c}} \overline{\sigma\phi_2^2}\gamma_2\chi_2 + \overline{\sigma\hat{\phi}_3^2}\nabla\Phi_3\cdot\nabla\chi_3 \\ &\qquad + \lambda_2\cdot\begin{pmatrix} \dfrac{\partial}{\partial y}\chi_2 - \dfrac{\partial}{\partial y}\chi_3 \\ \dfrac{\partial}{\partial x}\chi_3 - \dfrac{\partial}{\partial x}\chi_2 \end{pmatrix} + \begin{pmatrix} \dfrac{\partial}{\partial y}\gamma_2 - \dfrac{\partial}{\partial y}\Phi_3 \\ \dfrac{\partial}{\partial x}\Phi_3 - \dfrac{\partial}{\partial x}\gamma_2 \end{pmatrix}\cdot\kappa_2 \\ &= \int_{\Omega_{2\text{-D}}} \overline{\phi_2^2} \operatorname{curl}_{2\text{-D}} \mathbf{T}_2\chi_2 - i\omega\mu\mathbf{T}_2\cdot\kappa_2 \end{aligned} \tag{30}$$

for all $\chi_2, \chi_3 \in H^1(\Omega_{2\text{-D},c})$ and $\kappa_2 \in H_\lambda(\Omega_{2\text{-D},c})$.

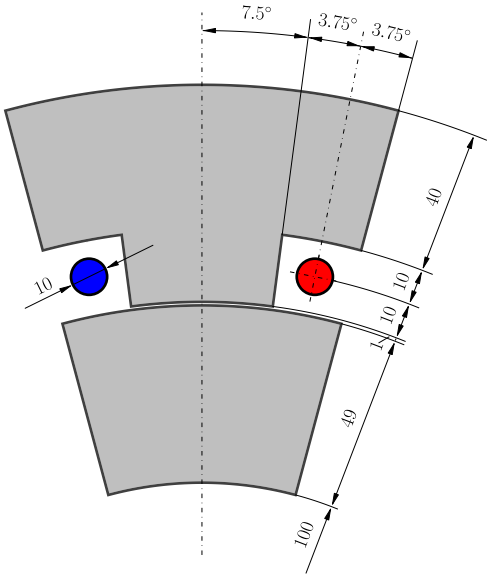

Fig. 1. One twelfth of a fictitious machine, consisting of steel sheets (gray) and air domains (left blank). Positive and negative sources are drawn in red and blue, respectively. All measurements are in mm. The thickness of the sheet is $d = 0.5$ mm with a fill factor of 0.95.

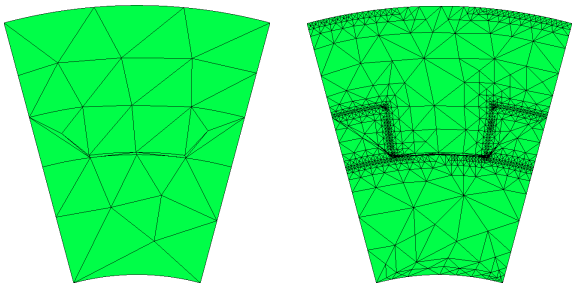

Fig. 2. Starting mesh (left) and the adaptively refined mesh after ten iterations (right).

Once all components are calculated, the total estimator can be evaluated on the 2-D mesh as

$$\begin{aligned}
&\|\sigma\gamma - \operatorname{curl}\mathbf{T}_{\text{2-D/1-D}}\|_\rho^2 \\
&\quad= \int_{\Omega_{\text{2-D},c}} \overline{\sigma\hat{\phi}_1^2}\nabla\Phi_1\cdot\nabla\Phi_1^* + \overline{\sigma\hat{\phi}_3^2}\nabla\Phi_3\cdot\nabla\Phi_3^* \\
&\qquad+ \overline{\sigma\hat{\phi}_1\hat{\phi}_3}\left(\nabla\Phi_1\cdot\nabla\Phi_3^* + \nabla\Phi_3\cdot\nabla\Phi_1^*\right) \\
&\qquad- \overline{\hat{\phi}_1^2}\left(\nabla\Phi_1\cdot\begin{pmatrix}-\mathbf{T}_{2,y}\\ \mathbf{T}_{2,x}\end{pmatrix}^* + \begin{pmatrix}-\mathbf{T}_{2,y}\\ \mathbf{T}_{2,x}\end{pmatrix}\cdot\nabla\Phi_1^*\right) \\
&\qquad- \overline{\hat{\phi}_1\hat{\phi}_3}\left(\nabla\Phi_3\cdot\begin{pmatrix}-\mathbf{T}_{2,y}\\ \mathbf{T}_{2,x}\end{pmatrix}^* + \begin{pmatrix}-\mathbf{T}_{2,y}\\ \mathbf{T}_{2,x}\end{pmatrix}\cdot\nabla\Phi_3^*\right) \\
&\qquad+ \overline{\rho\hat{\phi}_1^2}\begin{pmatrix}-\mathbf{T}_{2,y}\\ \mathbf{T}_{2,x}\end{pmatrix}\cdot\begin{pmatrix}-\mathbf{T}_{2,y}\\ \mathbf{T}_{2,x}\end{pmatrix}^* + \overline{\sigma\phi_0^2}\gamma_0\gamma_0^* \\
&\qquad+ \overline{\sigma\phi_0\phi_2}\left(\gamma_0\gamma_2^* + \gamma_2\gamma_0^*\right) + \overline{\sigma\phi_2^2}\gamma_2\gamma_2^* \\
&\qquad- \overline{\phi_0\phi_2}\left(\gamma_0\operatorname{curl}\mathbf{T}_2^* + \operatorname{curl}\mathbf{T}_2\gamma_0^*\right) \\
&\qquad- \overline{\phi_2^2}\left(\gamma_2\operatorname{curl}\mathbf{T}_2^* + \operatorname{curl}\mathbf{T}_2\gamma_2^*\right) \\
&\qquad+ \overline{\rho\phi_2^2}\operatorname{curl}\mathbf{T}_2\operatorname{curl}\mathbf{T}_2^*. \qquad (31)
\end{aligned}$$

The integrand can also be used locally to identify the finite elements with the highest contribution to the total error.

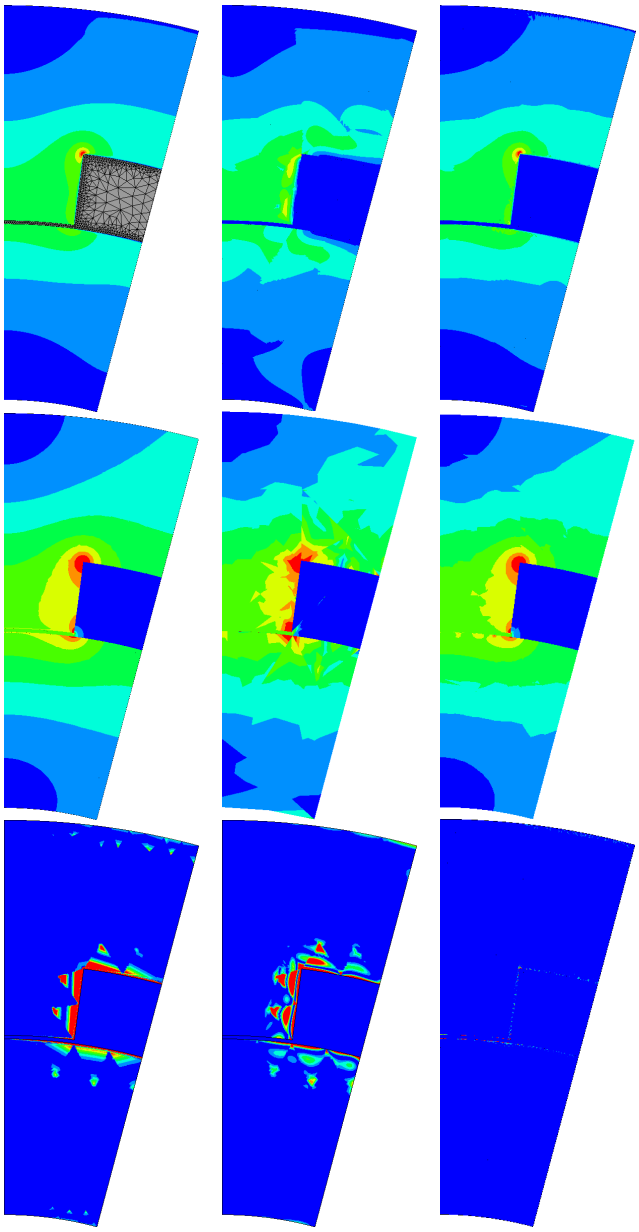

Fig. 3. First row: the absolute value of **J** drawn for the reference solution (left), the 2-D/1-D solution early in the refinement (middle) and at the end (right). Second row: the absolute value of **B** drawn for the reference solution (left), the 2-D/1-D solution early in the refinement (middle) and at the end (right). Third row: the local error early in the refinement (left) and the associated estimator (middle). The right figure shows the error at the end of the refinement. All figures in one row use the same relative color scheme. Only half of the domain is shown to preserve space.

V. Numerical Example

Consider the fictitious machine shown in Fig. 1. Using rotational symmetries, only one twelfth of the entire machine has to be simulated. For the steel sheet a magnetic permeability of $\mu = 1000\mu_0$ and an electric conductivity of $\sigma = 2.08$ MS is prescribed. The frequency is 50 Hz. The sources are not resolved in the finite element mesh and only included via their Biot-Savart fields.

All calculations were done using the open-source software Netgen/NGSolve [14]. This package has a python interface which naturally supports the input of the required

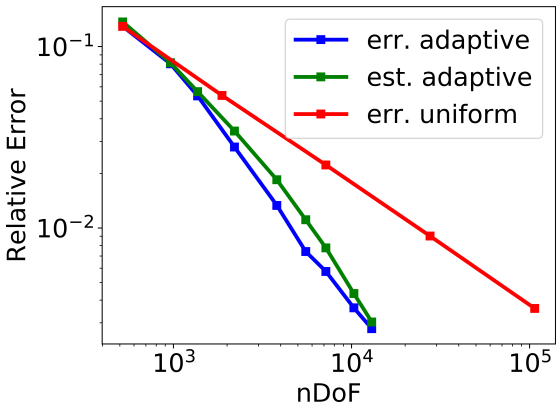

Fig. 4. Relative error, measured in the norm of the eddy current losses, relative to the required degrees of freedom, for both adaptive and uniform mesh refinement as well as the estimated relative error for the adaptive approach.

formulations (3), (8), (29) and (30), and the evaluation of arbitrary integrals like (31).

The calculations start with the coarsest possible mesh for the given geometry, see Fig. 2. In each iteration, the estimator is evaluated for each individual finite element. Then, all elements where this evaluation yields at least half of the maximum encountered estimator, are refined. In this process some adjacent elements might get refined as well in order to avoid hanging nodes.

As can be seen, the refinements are concentrated at the inner edges (due to the edge effect), at the corners (where the fields peak, see also Fig. 3) and at the inner and outer boundaries (where the boundary conditions need to be resolved correctly). Note also that almost no refinement happens along the vertical symmetry line where the fields are perfectly parallel and easy to resolve.

A qualitative evaluation of the estimator is shown in Fig. 3 where both the error and the estimator are depicted after two mesh refinements. All errors were calculated with respect to a numerical reference solution which has been calculated on a finely resolved 3-D mesh with higher order finite elements. It can be seen that the estimator correctly identifies the regions where the error is concentrated, further justifying the refinements.

Finally, as a quantitative evaluation Fig. 4 shows the relative error

$$\frac{\|\operatorname{curl}\mathbf{T}-\operatorname{curl}\mathbf{T}_{\text{2-D/1-D}}\|_\rho^2}{\|\operatorname{curl}\mathbf{T}\|_\rho^2} \tag{32}$$

of the 2-D/1-D MSFEM solution compared to the required degrees of freedom (nDoF) in the finite element problem for both adaptive refinement and uniform refinement. Of course, in a practical application, only the absolute error in the numerator of (32) can be estimated. Note also that the total error

$$\begin{aligned}&\|\operatorname{curl}\mathbf{T}-\operatorname{curl}\mathbf{T}_{\text{2-D/1-D}}\|_\rho^2\\&=\int_\Omega \rho(\operatorname{curl}\mathbf{T}-\operatorname{curl}\mathbf{T}_{\text{2-D/1-D}})\cdot(\operatorname{curl}\mathbf{T}-\operatorname{curl}\mathbf{T}_{\text{2-D/1-D}})^*\end{aligned} \tag{33}$$

is the integral over the local errors, i.e., it only becomes small if the fields are close to each other everywhere. This can also be seen in Fig. 3 where it is shown that the error becomes negligible compared to the starting error everywhere inside the domain.

As can be seen, the adaptive refinement leads to a great increase in the rate of convergence. After the final refinement the relative error for both the uniform and the adaptive method is below 0.5%. However, the adaptive method uses only about a tenth of the degrees of freedom. This makes the calculations drastically more computationally efficient. Furthermore, it can be seen that the estimator gives a good approximation of the behavior of the error with only a small overestimation.

VI. Conclusion

An a posteriori error estimator has been presented for the 2-D/1-D MSFEM **T**-formulation of the eddy current problem, based on the theory of flux equlibration. The estimator also utilizes a 2-D/1-D MSFEM approach in order to prevent its calculation costs to dominate the solution of the problem. Numerical examples show that it gives reliable estimates of the error in both a global and a local sense. This makes it an efficient tool for adaptive mesh refinement to increase the rate of convergence of the 2-D/1-D MSFEM solution.

Appendix
Shape Functions

Assuming that the sheet thickness is aligned with the z-axis, the definition of the shape functions uses the auxiliary scaling variable $s := (2z/d_{\text{Fe}})$, which transforms the arbitrary interval $[-(d_{\text{Fe}}/2), (d_{\text{Fe}}/2)]$ into the normalized interval $[-1, 1]$. The shape functions used in this article are given as

$$\phi_0(s) = 1 \tag{34}$$

$$\hat{\phi}_1(s) = \frac{d_{\text{Fe}}s}{2} \tag{35}$$

$$\phi_2(s) = \frac{1}{2}\sqrt{\frac{3}{2}}\left(s^2-1\right) \tag{36}$$

$$\hat{\phi}_3(s) = \frac{d_{\text{Fe}}\sqrt{6}}{8}s\left(\frac{s^2}{3}-1\right) \tag{37}$$

see also Fig. 5. In the insulation layer, ϕ_0 and ϕ_2 are extended by the constants 1 and 0, respectively. The functions $\hat{\phi}_1$ and $\hat{\phi}_3$ only appear in the definition for the estimator, which is only defined within the sheet.

In order to write the required integrals concisely, let κ be a generic material parameter that is equal to κ_{Fe} in the sheet and equal to κ_0 in the insulation. In the application κ takes the place of σ, ρ or μ as needed or it can be omitted by implicitly setting $\kappa_{\text{Fe}} = \kappa_0 = 1$. The integrals required for (8), (29), (30), and (31) are given by

$$\overline{\kappa\hat{\phi}_1^2} = \frac{d_{\text{Fe}}^3\kappa_{\text{Fe}}}{12} \tag{38}$$

$$\overline{\kappa\phi_2^2} = \frac{d_{\text{Fe}}\kappa_{\text{Fe}}}{5} \tag{39}$$

$$\overline{\kappa\phi_2'^2} = \frac{2\kappa_{\text{Fe}}}{d_{\text{Fe}}} \tag{40}$$

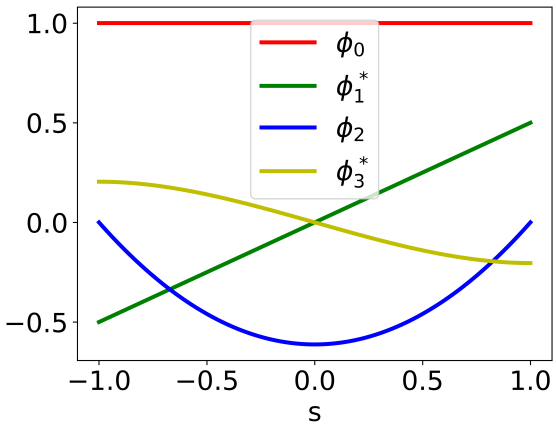

Fig. 5. Used shape functions $\phi_0, \hat{\phi}_1, \phi_2, \hat{\phi}_3$. Note that $\hat{\phi}_1$ and $\hat{\phi}_3$ are scaled to $d_{\mathrm{Fe}} = 1$ for better visibility.

$$\overline{\kappa\phi_0\phi_2} = -\frac{\sqrt{6}d_{\mathrm{Fe}}\kappa_{\mathrm{Fe}}}{6} \tag{41}$$

$$\overline{\kappa\hat{\phi}_3^2} = \frac{17d_{\mathrm{Fe}}^3\kappa_{\mathrm{Fe}}}{840} \tag{42}$$

$$\overline{\kappa\hat{\phi}_1\hat{\phi}_3} = -\frac{\sqrt{6}d_{\mathrm{Fe}}^3\kappa_{\mathrm{Fe}}}{60}. \tag{43}$$

The terms containing ϕ_0^2 are a special case and one has to differentiate between the integral over the entire domain including the sheet and the insulation and the integral over just the sheet. Therefore

$$\overline{\kappa\phi_0^2} = \kappa_{\mathrm{Fe}}d_{\mathrm{Fe}} + \kappa_0 d_0 \quad \text{in (8)} \tag{44}$$

$$\overline{\kappa\phi_0^2} = \kappa_{\mathrm{Fe}}d_{\mathrm{Fe}} \quad \text{in (29), (30) and (31).} \tag{45}$$

ACKNOWLEDGMENT

This research was funded in whole by the Austrian Science Fund (FWF) [10.55776/P31926]. For open access purposes, the author has applied a CC BY public copyright license to any author accepted manuscript version arising from this submission.

REFERENCES

[1] C. Jäger, I. Grinbaum, and J. Smajic, "Dynamic short-circuit analysis of synchronous machines," *IEEE Trans. Magn.*, vol. 53, no. 6, pp. 1–4, Jun. 2017.

[2] O. Bottauscio and M. Chiampi, "Analysis of laminated cores through a directly coupled 2-D/1-D electromagnetic field formulation," *IEEE Trans. Magn.*, vol. 38, no. 5, pp. 2358–2360, Sep. 2002.

[3] J. Pippuri, A. Belahcen, E. Dlala, and A. Arkkio, "Inclusion of eddy currents in laminations in two-dimensional finite element analysis," *IEEE Trans. Magn.*, vol. 46, no. 8, pp. 2915–2918, Aug. 2010.

[4] J. Gyselinck, R. V. Sabariego, and P. Dular, "A nonlinear time-domain homogenization technique for laminated iron cores in three-dimensional finite-element models," *IEEE Trans. Magn.*, vol. 42, no. 4, pp. 763–766, Apr. 2006.

[5] F. Henrotte, S. Steentjes, K. Hameyer, and C. Geuzaine, "Pragmatic two-step homogenisation technique for ferromagnetic laminated cores," *IET Sci., Meas. Technol.*, vol. 9, no. 2, pp. 152–159, Mar. 2015.

[6] M. Schöbinger, J. Schöberl, and K. Hollaus, "Multiscale FEM for the linear 2-D/1-D problem of eddy currents in thin iron sheets," *IEEE Trans. Magn.*, vol. 55, no. 1, pp. 1–12, Jan. 2019.

[7] P. Rasilo, E. Dlala, K. Fonteyn, J. Pippuri, A. Belahcen, and A. Arkkio, "Model of laminated ferromagnetic cores for loss prediction in electrical machines," *IET Electr. Power Appl.*, vol. 5, no. 17, pp. 580–588, 2011.

[8] K. Hollaus and M. Schöbinger, "Air gap and edge effect in the 2-D/1-D method with the magnetic vector potential *A* using MSFEM," *IEEE Trans. Magn.*, vol. 56, no. 1, pp. 1–5, Jan. 2020.

[9] M. Schöbinger, J. Schöberl, and K. Hollaus, "An equilibrated error estimator for the multiscale finite element method of a 2-D eddy current problem," *IEEE Trans. Magn.*, vol. 57, no. 6, pp. 1–4, Jun. 2021.

[10] O. Bíró, "Edge element formulations of eddy current problems," *Comput. Methods Appl. Mech. Eng.*, vol. 169, nos. 3–4, pp. 391–405, Feb. 1999.

[11] K. Hollaus and M. Schobinger, "A mixed multiscale FEM for the eddy-current problem with T, $\phi - \phi$ in laminated conducting media," *IEEE Trans. Magn.*, vol. 56, no. 4, pp. 1–4, Apr. 2020.

[12] J. Schöberl and S. Zaglmayr, "High order Nédélec elements with local complete sequence properties," *COMPEL Int. J. Comput. Math. Electr. Electron. Eng.*, vol. 24, no. 2, pp. 374–384, Jun. 2005.

[13] D. Braess and J. Schöberl, "Equilibrated residual error estimator for edge elements," *Math. Comput.*, vol. 77, no. 262, pp. 651–673, Nov. 2007.

[14] J. Schöberl. *Netgen/NGSolve*. Accessed: Mar. 13, 2024. [Online]. Available: https://ngsolve.org/